Plenary Lecture presented at the
12th International Conference on Plasma Surface Engineering (PSE 2010)
September 13-17, 2010, Garmisch-Partenkirchen, Germany

Manuscript submitted to
Surface and Coatings Technology
October 13, 2010

Discharge Physics of High Power Impulse Magnetron Sputtering

André Anders
Lawrence Berkeley National Laboratory, University of California, 1 Cyclotron Road, Berkeley, California 94720, USA

ACKNOWLEDGMENT

Technical support by Günter Mark of Melec GmbH and Joe Wallig of Berkeley Lab is gratefully acknowledged. Joakim Andersson, David Horwat, Sunnie Lim, Jason Sanders, and Rueben Mendelsberg have been involved in experiments and/or discussions; Jonathan Slack kindly supplied figure 1. This work was supported by Berkeley Lab's LDRD program, and by the U.S. Department of Energy under Contract No. DE-AC02-05CH11231.

Discharge Physics of High Power Impulse Magnetron Sputtering

André Anders
Lawrence Berkeley National Laboratory, University of California, 1 Cyclotron Road, Berkeley, California 94720, USA

Abstract

High power impulse magnetron sputtering (HIPIMS) is pulsed sputtering where the peak power exceeds the time-averaged power by typically two orders of magnitude. The peak power density, averaged over the target area, can reach or exceed 10^7 W/m^2, leading to plasma conditions that make ionization of the sputtered atoms very likely. A brief review of HIPIMS operation is given in a tutorial manner, illustrated by some original data related to the self-sputtering of niobium in argon and krypton. Emphasis is put on the current-voltage-time relationships near the threshold of self-sputtering runaway. The great variety of current pulse shapes delivers clues on the very strong gas rarefaction, self-sputtering runaway conditions, and the stopping of runaway due to the evolution of atom ionization and ion return probabilities as the gas plasma is replaced by metal plasma. The discussions are completed by considering instabilities and the special case of "gasless" self-sputtering.

1. Introduction

Derived from a Plenary Talk at the 2010 Plasma Engineering Conference, this work is limited to a brief recap of sputtering basics followed by considerations of how the magnetron operates under high power pulsed conditions. The emphasis will be on the ionization of sputtered atoms followed by self-sputtering, which may or may not amplify to result in self-sputtering "runaway". The runaway phenomenon will be illustrated by new data related to its onset and the establishment of sustained, steady-state self-sputtering. For simplicity and transparency, and given the finite space, the considerations are mostly phenomenological and limited to non-reactive sputtering using pure argon or krypton.

High power impulse magnetron sputtering (HIPIMS) is a relatively young physical vapor deposition (PVD) technology that combines magnetron sputtering with pulsed power technology [1-3]. The objective is to achieve ionization of the sputtered atoms in order to have ions available for substrate etching (pre-treatment) [4] and/or for assistance to the film growth process, leading to well-adherent coatings of desirable microstructure and properties [5].

In contrast to conventional mid-frequency pulsed sputtering, the power densities during pulse on-time are much higher in HIPIMS. To clearly define the scope, two definitions of HIPIMS are offered here. First, a technical definition could be "*HIPIMS is pulsed sputtering where the peak power exceeds the time-averaged power by typically two orders of magnitude.*" This definition implies that long pauses exist between pulses of very high amplitude, hence the word "impulse" is justified in the terminology. The peak power density, averaged over the target area, often exceeds 10^7 W/m^2. Alternatively, one could consider the more physical definition "*HIPIMS is pulsed sputtering where a very significant fraction of the sputtered atoms becomes ionized*." This definition implies that self-sputtering occurs, which may or may not be exclusively sustained by target ions.

2. A brief recap of sputtering basics

Sputtering has a very long history that can be traced back to the mid 19th century [6]. William Grove [7] is attributed to be the first who reported on the formation of deposits when investigating the electrical properties of gases at low pressure. Interestingly, given the limited availability of electrical power to do experiments, it was common to make use of primary cells in conjunction with inductors, i.e. using Faraday's principle of inductive generation of high voltage pulses via repetitive current interruption. Therefore, all original experiments of sputtering of the mid and even late 19th century were *pulsed*. Arthur Wright, for example, used pulsed sputtering to produce films of numerous elements and investigated their stability when exposed to the atmosphere [8]. Films tended to be porous since sputtering involved relatively high pressure (by today's standards). Higher quality films are made at much lower pressure, of order 1 Pa or less, when one could make use of the energetic particles that originate from the cathode in the sputtering process. Going to lower pressure, however, had practical limits. First, adequate pumps were required and, once lower pressure *was* reached, the discharge ceased to work as the mean free path for ionizing collisions exceeded the electrode distance.

The solution to low pressure operation was found by trapping and "recycling" the energetic particles (i.e. electrons in the case). Particle trapping can be done electrostatically with oppositely positioned cathode sheaths forming a hollow cathode (e.g. [9]). Another approach is with pure magnetic mirroring [10], which was considered for thermonuclear fusion. Finally one could use a combination of electric and magnetic fields, which was introduced by Frans Penning, who invented the Penning trap and the basic magnetron principle [11]. The breakthrough for industrial coatings came with the development of the planar magnetron in the 1970s. This is the basic configuration we are considering here (Fig. 1), although the cathode of the discharge (target) can have other forms like an elongated slab, or a cylinder.

The magnetron discharge is a clever, magnetically enhanced glow discharge characterized by a closed drift of electrons. The actual electron path is very complicated due to the presence of non-uniform electric and magnetic fields. Neglecting for a moment the electric field, an electron will gyrate in the magnetic field with the cyclotron frequency

$$\omega_e = eB/m_e \tag{1}$$

where B is the magnetic inductance, e is the elementary charge and m_e is the electron mass. An electron having a velocity component $u_{e\perp}$ perpendicular to the field vector $\mathbf{B}$ will have a gyration radius

$$r_{g,e} = \frac{u_{e\perp}}{\omega_e} = \frac{m_e u_{e\perp}}{eB}. \tag{2}$$

The gyration is sometimes referred to as the *cyclotron motion*. Typically, the electron will gyrate many times around a magnetic field line before colliding with another particle. The cyclotron motion is therefore largely bound to the magnetic field line, which is considered the "magnetization" of the electron motion. It is practical to average over the gyration motion and consider the motion of the gyration center rather than the motion of the electron itself [10].

Now, adding an electric field by applying a voltage between anode and cathode, each cyclotron revolution is associated with an acceleration and deceleration. The gyration path is not quite circular anymore, which leads to a net drift perpendicular to both $\mathbf{B}$ and $\mathbf{E}$ field vectors. This is known as the $\mathbf{E}\times\mathbf{B}$ drift [10] (of the gyration or "guiding center"). Considering the planar magnetron geometry shown in Fig. 1, the drift is in the azimuthal direction and closed, i.e. the trapping and "recycling" of the electron is accomplished. The closed drift of electrons is

sometimes referred to as the *magnetron motion*, and the associated azimuthal electric current is also described as the Hall current. For typical operation of a direct current (DC) magnetron, the Hall current exceeds the discharge current by roughly one order of magnitude [12].

The electric field between the cathode (negative) and anode (positive) is highly non-uniform. Once the discharge plasma is established, most of the voltage drop of typically several hundred volts will be located in the space-charge layer, known as the sheath, adjacent to the target surface. Only roughly 10% of the voltage will drop outside the sheath, and the actual distribution will depend on the magnetic field and discharge conditions. The implication is that (i) electrons gain most energy when crossing the sheath coming from the target surface (i.e. the secondary electrons are the most energetic), and (b) plasma electrons, which have typically only a few eV of energy, cannot penetrate the sheath but "bounce off" and return to the plasma.

The magnetic field is also highly non-uniform (Fig. 1). Magnetic mirroring, a consequence of magnetic moment conservation, may occur as the electron gyration center follows the field line into a region of increasing field [10] (an increasing magnetic field is illustrated by an increase in the density of magnetic field lines, as done in Fig. 1). Furthermore, those electrons that manage to approach the sheath will be reflected at the sheath edge. One may therefore state that the pendulum-like motion of the electron gyration center is an effect of magnetic mirroring and reflection by the electric field.

Ions are generally not magnetized in sputtering magnetrons since their gyration radius usually exceed the characteristic system length. Ions are accelerated by the electric field: positive ions towards the target, and negative away. Sputtering of surface atoms from the target is really based on the last "kick" that positive ions obtain in the sheath before impacting the target surface.

3. Operation of a magnetron with high power pulses

3.1 A brief overview

There have been several publications on high power pulsed glow and magnetron discharges in the 1990s [13-15], though the field of HIPIMS took off only after the seminal paper by Kouznetsov *et al.* [1], as evident by the many publications since, and the introduction of first industrial applications.

Before discussing the effects of high power, let's have a look at an initial motivation for pulsing a magnetron discharge. Glow discharges in general, and magnetron discharges in particular, have a propensity to "arcing" [16]. The arc is here an unwanted mode of discharge, typically associated with high currents and low voltages, and characterized by the formation of cathode spots on the target which, most annoyingly, emit microscopic droplets that spoil the quality of coatings [17]. In the 1990s it was shown that the probability of forming an arc could be greatly reduced by using mid-frequency pulsed sputtering [18-19]. The issue is even more important when higher currents are used, like in HIPIMS. Modern HIPIMS power supplies are equipped with arc detection and suppression (a short interruption of the process when an arc is detected). However, even with arc suppression in place, the brief period of an arc's existence before suppression may be detrimental to the coating quality. It would be desirable to establish a process where arcing is very unlikely. One approach is derived on the strategy of using short (< 50 μs) pulses, which worked so well for mid-frequency sputtering [19] since arc spots tend to develop with some delay in the presence of plasma. In the short pulse case, the shape of the current pulses is approximately triangular since the current has not reached the maximum that

could develop for the given voltage [20-21]. The plasma density is increasing and the impedance falling as the pulse progresses. The peak current or peak current density is sometimes used to characterize the plasma properties and resulting film microstructure (e.g. [22-23]). However, from a physics point of view, energy (but not current) is a conserved quantity, and therefore the power density is a more general parameter, which many researchers prefer to use when describing the discharge-film properties relationships (e.g. [20, 24-27]).

The fact that the discharge current has not yet reached its maximum with short pulses suggest indicates that longer pulses, which can be sustained without arcing in most cases, should be explored [21]. Longer pulses (~ 1 ms) will clearly show the effects of dynamic gas rarefaction and self-sputtering, which are discussed in sections 3.3 and 3.4, respectively. Longer pulses of even several milliseconds have been demonstrated using pulse shaping, where the high power portion of each pulse follows a pre-pulse of much lower power. This approach has been termed Modulated Pulsed Power (MPP) [28]. The MPP technology has been shown to have advantages for process control, especially for the reactive deposition of compound films.

3.2 Delay of current onset

In this and the following sections, HIPIMS discharges are considered in their simplest form where pulses are repetitively applied without having any pre-pulse or underlying low-power DC discharge. In this case one observes a more or less significant delay of the current rise with respect to the application of the voltage pulse. For example, a long delay of 50 μs was shown in Fig. 1 of the seminal paper by Kouznetzov and colleagues [1]. In a recent study of this phenomenon [29], it was shown that the current onset can be described by extending much earlier considerations of glow discharge onset, and specifically those by Schade [30]. The time delay, t_d, can generally be thought of being composed of a *statistical time lag*, t_s, for the initial electrons to appear in the electric field between electrodes, and a *formative time lag*, t_f, corresponding to the time required for the discharge to develop from the initial electrons:

$$t_d = t_s + t_f . \tag{3}$$

In most cases, initial "seed" electrons are present, for example those left over from a previous pulse, and therefore the statistical time lag is in most case negligibly small: $t_s \ll t_f$. The formative time lag was shown to be caused by the time ions need to reach the target,

$$t_i = \sqrt{\frac{2s}{E}\frac{m_i}{q_i}} , \tag{4}$$

plus the time the secondary electrons need to cause ionization of the gas,

$$t_e \approx \left(\frac{m_e}{2E_e}\right)^{1/2} \frac{kT_a}{\sigma_{ea}\left(E_e\right) p}, \tag{5}$$

with the cycle of ionization and secondary electron generation repeating several times until a plasma is produced and a measurable current can be recorded [29]. In deriving the equations it was assumed that the electric field E is not yet much redistributed by the space charge of the developing sheath near the target, and the symbols have the following meaning: s is a typical distance between the location of ionization and the target surface, q_i is the electric charge of the ion, E_e is a characteristic energy gained by the electron from the electric field, m_e is the electron mass, $T_a \approx 300$ K is the gas temperature, k is the Boltzmann constant, p is the pressure, and

$\sigma_{ea}(E_e)$ is the ionization cross section which depends on the relative velocity of the electron and atom, i.e. essentially on the electron energy.

The formative time lag can practically be eliminated when not just *some* initial electrons are present but an appreciable plasma density *before* the HIPIMS pulse is applied; this can be realized by using a low power DC "simmer" discharge, or a low power pre-pulse phase [31], or the tailored pre-pulse realized in the MPP technology [28, 32], or by injecting pulsed thermionic arc plasma [14], or cathodic arc plasma [33].

3.3 Gas rarefaction and sputter wind

The flux of sputtered atoms and reflected ions (now atoms) from the target has an appreciable effect on the gas in front of the target because, through collisions, the gas will be locally displaced and heated, and its density greatly reduced. This has already been recognized by Steenbeck in the late 1920s when he investigated the ignition of pulsed glow discharges [34]. The reduction of the gas density has been termed *rarefaction*, and clearly it is very important for the discharge since a local reduction of gas density is (partially) equivalent to reducing the original gas pressure.

Rarefaction has been investigated for DC magnetron sputtering [35-39] and one should expect that the effect is much greater in HIPIMS, which indeed it is. Sputtered atoms have typically several eV of kinetic energy when leaving the target. Following the Sigmund-Thompson theory [40-41], the energy distribution function can be approximated by [42]

$$f_{\text{Thompson}}(E) \propto \frac{E}{(E+E_{SB})^3} \tag{6}$$

where the surface binding energy E_{SB} is an important material parameter. Even with the relatively modest flux of atoms in the case of DC sputtering, the reduction of gas density in front of the target is significant, especially when relatively high gas pressure is used [37]. For example, Rossnagel found a reduction down to about 25% of the original gas density when sputtering copper using a power of up to 3 kW on a 15 cm diameter target in argon [35-36]. Using his data and making a bold extrapolation to higher, typical HIPIMS peak powers (Fig. 2), we see that the gas is likely to be pushed away very strongly and one should expect that copper practically replaces the gas. This has been confirmed using optical and particle spectrometries, or simply by looking at the independence of the discharge current on pressure at later times in the discharge pulse (e.g. Fig. 2 of [43] and more recently in [44]). Gas rarefaction readily explains the initial target current peak seen when using relatively long pulses at low and modest power densities, like the one shown for copper HIPIMS in Fig. 1 of [43], and for niobium in Fig 3.

There are many features of the curves in Fig. 3 that deserve consideration. First, looking at the current pulse recorded 30 seconds after the start of HIPIMS pulsing, we see a delay of about 20 μs of current onset with respect to the application of the voltage pulse, which is defined as time zero. This delay was discussed in section 3.2. Second, we see the initial current rise to 32 A followed by a large reduction to about 10 A, which can be associated with the reduction of argon ion production since the argon atoms are pushed away by the "sputter wind" (a term coined by Hoffman in 1985 [45]). The target or discharge current is composed of the ion current to the target and the current of secondary electrons from it,

$$I = I_i + I_{SE} = (1+\gamma_{SE}) I_i , \tag{7}$$

where γ_{SE} is the yield of secondary electrons. This yield will be discussed later in section 3.5, and here we note only that γ_{SE} is typically 0.1 or smaller, and hence by far most of the recorded target current is ion current. With the reduction of the ion current by rarefaction, the "sputter wind" is also reduced. Therefore, it is not surprising that the gas starts to refill the low-density zone in front of the target. This, in turn, allows more ionization processes to occur and the ion current to the target can increase again. For certain combinations of gas pressure and power one can observe slow and large oscillations associated with pressure waves caused by a modulated sputter wind.

Pressure and plasma density waves have been observed before in HIPIMS systems [46]. In some cases one sees only one pulse propagating, resembling a solitary wave [47], which is most likely caused by the switch-on of the "sputter wind".

The initial current peaks of the curves labeled "after 60 s" and "after 90 s" are smaller than the peak "after 30 s". This can also be explained by rarefaction, though this time taking into account the increasing temperature of the target surface. The argon gas density decreases according to the ideal gas equation

$$n_a = p/kT_a \tag{8}$$

which can be used to estimate the situation keeping in mind that the large chamber (here 200 liters) ensures a constant average pressure. The gas in the vicinity of the target surface is heated, and according to (8), its density is decreased compared to other locations of the chamber and compared to the initial conditions when the target was still at room temperature. Less gas density leads to a small gas ion flux to the target, i.e. lower current.

There is plenty of evidence that the target surface gets very hot in HIPIMS processing. First, timescales of many seconds, or minutes, are indicative for a thermal process since all other processes tend to be much faster. One could solve the heat conduction equation for the target, with the cooled side as one boundary condition and ion bombardment heating on the other side to confirm such timescales. Experimentally, under conditions of high power and long pulses, target glow can be seen when the process is stopped after operating for a minute or longer. In case of magnesium, aluminum, bismuth and zinc targets one finds that the used target surface exhibits very large grains indicative of high-temperature grain growth. In extreme cases one can also find evidence of melting, like for the copper target shown in Fig. 4. In fact, target cooling is a main limitation in using very long pulses at very high power.

Returning to Fig. 3, we see that the current pulses change in a matter of about one minute, which in part can be explained by gas rarefaction, but one also sees the growth of current, especially later in the pulse. The current amplitude goes beyond the initial peak, which is indicative that not only argon ions but ionized target atoms play an important role. In fact, the curves of Fig. 3 were taken right at about the threshold to self-sputtering runaway, which will be explained next.

3.4 Self-sputtering runaway

The main objective of applying high power pulses is to ionize the sputtered atoms. Doing so implies that the newly born ions will participate in the sputtering process, i.e. ions of the target material will sputter the target material, which is called self-sputtering. This process has been well known for a number of years. In 1980, Hosokawa and colleagues [48] pointed out that, under certain conditions, self-sputtering can operate in a self-sustained mode, namely when ions of the target material are created at a sufficient rate such that the process gas becomes

unnecessary. They showed that once the high power sputtering discharge has started, the argon gas can be switched off and the discharge will remain. That works well for copper, a material of very high self-sputter yield, and for a few other high yield materials.

The condition for sustained self-sputtering can be written as [48]

$$\Pi \equiv \alpha\beta\gamma_{SS} = 1 \tag{9}$$

where α is the probability that a sputtered atom becomes ionized, β is the probability that the newly formed ion returns to the target, and γ_{SS} is the self-sputtering yield. Before a steady-state condition according to (9) establishes itself, a transient phase of self-sputtering runaway occurs, characterized by $\Pi > 1$. In [21, 43] it was shown that runaway occurs at a very well-defined threshold power, set by the applied voltage. Runaway can be readily obtained for copper and other high yield materials, such as silver and zinc, though it is much more involved for others, like the transition metals.

Runaway is understood intuitively by remembering that the more atoms are sputtered the more can be ionized; and the more ions are formed and return to the target the more atoms can be sputtered. This loop is illustrated in Fig. 5. Since $\alpha < 1$ and $\beta < 1$, the condition $\gamma_{SS} > 1$ is necessary but not sufficient for runaway and sustained self-sputtering.

The runaway cycle, Fig. 5, can amplify itself until some limitation kicks in. For example, the limitation could be the power supply: the voltage will droop, followed by a reduction of current. If the power supply could deliver the high current as required by the falling impedance, then other, non-technical but physical limits will appear. Looking at Fig. 5, the two obvious loss terms are the fluxes of atoms and ions to the substrate (or elsewhere), though other, perhaps more important factors are the changes of $\alpha(t)$ and $\beta(t)$ as the runaway progresses, which will be discussed in the next sections.

For now, we illustrate the runaway with an example. While most work in the literature of self-sputtering runaway deals with high yield materials like copper, the situation will be illustrated here with the self-sputtering of niobium, a material selected for its practical importance as well as to show that transition metals can exhibit the features of self-sputtering. Fig. 6 shows the case of niobium sputtering with 0.25 Pa of argon present. When a voltage pulse of 510 V is applied the discharge barely starts: it takes a very long time (260 μs) before the current pulse is visible. One sees the familiar initial peak followed by rarefaction to steady state of a bit less than 10 A. Higher applied voltages reduce the delay, and interesting waves and features appear as we approach the runaway threshold. At 570 V, runaway to much higher currents can bee seen with a great delay of about 700 μs. Clearly, there is no "in-between" state: the current is either sub-threshold, $\Pi < 1$, or a temporary runaway happened, $\Pi > 1$, until the current settles at a high level steady state where $\Pi = 1$ must hold.

3.5 The evolution of the secondary electron emission and ionization probability

The ionization probability is closely related to the energy of electrons, which in turn is mainly determined by the emission of secondary electrons. The rather abrupt transition from runaway (increasing current and $\Pi > 1$) to a steady-state situation (constant current and $\Pi = 1$) requires that α and other parameters change. For example, looking at the currents for the higher voltages in Fig. 6, or the current in Fig. 7, taken 10 s after starting the pulsing experiment, we see a very sudden change from strongly rising current to approximately constant current.

As mentioned in section 2, secondary electrons are a major supplier of energy to the plasma because they gain much energy when passing through the electric field of the target sheath. This

energy (in eV) can be as high as 80-90% of the applied voltage (in V) and is therefore capable of causing many ionization processes, namely up to about $0.8\,eV_{pulse}/E_{0\to1} \sim 50$ per electron using an over-simplified energy estimate, where V_{pulse} is the applied voltage during the pulse, and $E_{0\to1}$ is the first ionization energy (Table 1). Secondary electrons are therefore a critical "engine" for the HIPIMS discharge [49]: they facilitate electron heating and electron impact ionization. If the supply of secondary electrons is reduced, it will immediately reduce the energy supplied to the plasma and the ionization rate will go down. Although detailed simulations still need to be done, it is clear that we have a critical physical "break" of the runaway process because singly charged metal ions have a very small secondary electron yield, which is perhaps the main physical reason that ends the self-sputtering runaway phase [49].

To elaborate on this, a closer look at the secondary electron emission process is needed. One generally distinguishes between kinetic and potential electron emission. For clean surfaces, *kinetic emission* (KE) is dominant when the primary ion energy exceeds about 300 eV/amu [50-51] and it can be observed down to an apparent threshold of about 10 eV/amu [52], which is about 400 eV for argon ions. For "dirty" or technological surfaces, the threshold is reduced by about one order of magnitude and the yields can vary greatly depending on the specifics of the surface [53]. Whether or not a target surface can be considered "clean" depends on the balance of target erosion and adsorption from the gas phase. For the relatively low kinetic energies of ions in magnetron sputtering we need to consider *potential emission* (PE), i.e. emission associated with the ionization potential of the arriving ion [52]. Experimental data of the secondary emission yields for various ions satisfy the fit [54]

$$\gamma_{SE} = 0.032\left(0.78\,E_{pot} - 2\phi\right), \tag{10}$$

which implies that the condition

$$0.78\,E_{pot} > 2\phi \tag{11}$$

needs to be fulfilled for PE to occur; here E_{pot} is the potential energy, which for most ions is the first ionization energy: $E_{pot} = E_{0\to1}$, and ϕ is the work function. A closer look at the work functions and first ionization energies of metals (Table 1) shows that condition (11) is not fulfilled for singly charged metal ions (this statement is also true for metals not shown in Table 1).

We note that the first ionization energy of argon or krypton is sufficiently high to satisfy condition (11). The gas plasma is replaced by the metal plasma as the self-sputtering runaway phase progresses, and hence the flux of secondary electrons may be greatly reduced. Secondary electron emission does not completely cease because some noble gas ions, some doubly charged metal ions, and UV photons arrive at the target surface and cause emission. The supply of energy to the plasma is reduced. Additionally, we should also look at how the available energy is distributed by considering the electron energy distribution function (EEDF). Gudmundsson and coworkers [55] showed that the electrons of the dense HIPIMS plasma have an EEDF that is close to Maxwellian, which is in contrast to DC magnetron plasmas where a Maxwellian and a group of higher energy electrons exist [56]. Impact ionization is the dominant ionization mechanisms, facilitated by the most energetic electrons of the distribution. With an increasing supply of neutral atoms by sputtering during the runaway, the electron temperature is reduced, which further limits ionization events, hence $\alpha(t)$ is reduced as runaway evolves.

3.6 The evolution of the return probability

Most ionization events occur in the region where the energetic electrons are trapped, i.e. where the magnetic field lines arch over the target. This is the region of the magnetic presheath. It has a significant electric field that accelerates ions towards the target. The formation of the sputtering "racetrack" is evidence for such preferred zone of ionization and ion guidance. The return probability β is therefore close to unity for ions formed near the target. Only ions formed in some distance from the target surface can escape. The escape probability of an ion from the target zone, $1-\beta$, is promoted by the initial kinetic energy that the atom had before ionization, namely from the sputtering process (equation (6)).

When a copper HIPIMS discharge surpassed the self-sputtering threshold (9) and runs away, no large jump was observed at the substrate [21], which indicated that the newly formed ions have a high probability to return to the target, i.e. β is close to unity. However, as the discharge was driven far beyond the runaway threshold, the ion flux to the substrate became very large [57], and the return probability was shown to be less than 50%. Clearly, the return probability is determined by the discharge conditions and will evolve as the system is in its runaway phase.

Recent measurements of the ion kinetic energy for the gasless case, which is briefly discussed in a later section, indicate that the potential distribution shifts and a highly asymmetric potential hump exists [58]. This hump can be considered like a "watershed" for the ion direction. Apart from a correction due to the "sputter wind", ions formed between the target and the hump are accelerated back to the target, while ions formed beyond the hump are slightly accelerated *away* from the target: they escape and participate in the thin film deposition process. The position and height of the potential hump will self-consistently form depending on the discharge conditions.

3.7. Sustained self-sputtering

The preliminary measurements suggest that the position of the hump is self-regulating for the HIPIMS discharge in its steady-state phase, when $\Pi = 1$. The relative stability of sustained self-sputtering is due to a negative feedback. Suppose we have a fluctuation to less sputtering. This will lead to less electron cooling, followed by stronger excitation and ionization producing singly and some doubly charged ions. This, in turn, enhances sputtering, thereby counteracting the initial disturbance. A fluctuation to higher sputtering is also accordingly dampened.

A similar consideration can be done for the return probability. The potential distribution in the magnetic presheath is affected by the plasma itself. Greater plasma density implies thinner sheath [59-62] and the potential hump is likely to shift closer to the target, allowing more ions to escape from the ionization region. Conversely, if there is a fluctuation to lower plasma density, the hump will shift away, "catching" more ions to be drawn back to the target.

Figure 7 shows another example of the interplay of rarefaction, runaway, and establishment of sustained self-sputtering. One can see that slow, thermal effects can greatly determine the behavior near the runaway threshold. In contrast to Fig. 3, this time the voltage is sufficient to facilitate runaway, at least in the beginning, as shown with the curve "after 10 s". Continued pulsing, though, makes the target hot and rarefies the argon gas, leading to less ion bombardment and sputtering, until runaway is completely suppressed. The great importance of the argon gas is associated with its contribution to secondary electron emission. Less argon does not only imply less sputtering but also less energy input to the plasma by a reduced flux of energetic secondary electrons.

3.8 Waves and instabilities

The magnetron plasma is subject to non-uniform electric and magnetic fields, with the electrons crossing magnetic field lines to reach the anode. It is actually surprising that the system works at all, especially under HIPIMS conditions, since the discharge current is greater than classical or Bohm transport predicts [63]. Even as Bohm diffusion across magnetic field lines is known to be based on microinstabilities, the observations of greater currents suggest that the plasma is turbulent. We should expect to find fluctuations, waves, and instabilities considering that we deal with several counter-streaming "fluids", namely a flux of positive ions to the target, a flux of neutrals from the target, a flux of electrons from the target to the anode, strong $\mathbf{E} \times \mathbf{B}$ drift and other drifts associated with non-uniformity of magnetic and electric fields. We should recall Maxwell's equations which tell us that moving charged particles are sources of electromagnetic fields, which add to the externally applied fields. Hence, it is surprising how well the system generally behaves.

Waves and instabilities have been reported in the literature. For example, Bugaev found slow instabilities in the recorded voltage when the current level exceeded about 400 A [14], and Gudmundsson and colleagues [46] found oscillations of the electron density at a relatively low frequency of 12.5 kHz even quite long after the HIPIMS pulse was terminated. Such fluctuations have also been observed by Sheridan and Goree [64] but they concluded that low-frequency turbulence is not responsible for cross-field electron transport.

Lundin and coworkers [63] studied oscillating electric fields in the megahertz range for HIPIMS plasmas using an array of electric field probes. They assign fast oscillations to a modified two-stream instability, which is known to enhance electron transport across the magnetic field lines.

The field of waves and instabilities in HIPIMS plasmas is far from being fully explored and understood. On the one hand, as mentioned before, those phenomena are essential to allow for high currents to exist. On the other hand, they may cause harm to the equipment and may disrupt the process. Fig. 7 shows an example of a low frequency instability: consider the current pulse labeled "after 10 s" in Fig. 7. The oscillations can be found in both current and voltage (Fig. 8) albeit with different frequencies. There are a few interesting features. The current shows at the end of the runaway phase a peak followed by a small reduction, which we know is associated with rarefaction of the gas. As the plasma contains less argon, the voltage suddenly becomes noisier. The current develops a wave of much slower frequency, with growing amplitude: an instability. Here we should mention that the voltage is measured at the power feedthrough to the target, and the target is separated by the cable inductance from the very large capacitance of the SPIK pulser.

Instabilities are essential to the operation; they may not only facilitate current transport but contribute to the generation of multiply charged ions in HIPIMS plasmas [65] and to the enhancement of gas dissociation and ionization should a reactive gas be present [28, 66].

3.9 Another example showcasing the interplay of rarefaction, runaway, and energy balance issues

Operating near the self-sputtering runaway threshold can shed more light on the critical processes of HIPIMS operation, and therefore another example is shown in Fig. 9. At relatively low voltages, 490 V or less, we see the usual sub-threshold current, characterized by a transient

peak at the beginning, transitioning to what could be DC operation if the pulse went on and target cooling was sufficient. At higher voltage, 500 V, the system runs away but, as the current level of about 50 A is reached, the discharge "chokes", which very likely can be assigned to the replacement of argon by metal and the associated reduction in secondary electron supply. After this episode, for $t > 500$ μs, the target surface is hot and the gas density does not go back to its original value, and hence no further runaway occurs. Practically the same happens at 510 V. At 520 V though, more energy is pumped into the system and the runaway finds conditions to stabilize at a high, self-sustained level. This is the lowest voltage at which sustained self-sputtering of niobium has been observed. Going to higher voltages, like 530 V and 540 V, gives a surprising delay of the onset of self-sputtering. Here we have to recall that those current curves were taken 30 s after starting a pulsing experiment. Once the current was recorded, the system was shut down and let cool down a few minutes before starting the next pulsing cycle. The delay observed for 530 V and 540 V can therefore be assigned to a rarefaction effect, namely the rarefaction caused by heating of the target in the first 30 s before the current was recorded. Another argument for rarefaction before the pulse is that the initial peak for 540 V is slightly lower than for 530 V. At even higher voltages, 550 V and higher, the supply of energy is sufficient and the system runs right away to reach the sustained self-sputtering conditions. Near the end of the 1 ms pulse we again see instabilities developing.

3.10 Sputtering with krypton

All results so far discussed in this contribution were obtain with argon, the most popular sputtering gas for its combination of physical and chemical properties and its relatively low cost. Krypton is sometimes used for its greater atomic mass and size compared to argon, which leads to lower gas incorporation and may have beneficial effects on the kinetics of film growth. HIPIMS behavior in krypton is generally similar to when argon is used, although there are some differences. Fig. 10 shows examples of the current pulse shape near the runaway threshold for two different pressures of krypton using the same niobium target. To limit the amount of data, only those curves are shown that were taken 30 s after a start of an experiment. Several minutes passed between experiments to let the target cool down to about room temperature.

The top part of Fig. 10 shows the current pulse with a background of 0.5 Pa of krypton. One can recognize all the features previously discussed. The current pulse shape for 540 V indicates self-sputtering but the situation is not well "decided": the system may run away to the typical higher level of almost 100 A, or it may choke — like what happened with the current pulses for 500 V and 510 V shown in Fig. 9. While the features shown in those single-shot recordings are typical, the curves right at the threshold, here 540 V, vary greatly from pulse to pulse. This again can be associated with the target temperature and its effect on gas density for the following pulse. Should runaway happen, more power is dissipated, the target surface temperature goes up and the gas density goes down, which will hamper the transition to runaway in the next pulses. As the surface temperature of the target is reduced, the gas density in front of the target increases and the system tends to runaway in the next pulses.

Looking now at the lower part of Fig. 10, where krypton has a pressure of 1.0 Pa, we can see a quite modified behavior near the threshold: clearly, the gas plays a greater role. Krypton has a mass comparable to niobium (Table 1), whereas argon is less than half as heavy. The mass ratio greatly affects the momentum transfer in collisions. Krypton has therefore a greater "stopping power" for the sputter wind compared to argon. Another factor is that krypton has slightly lower

ionization energies, which according to (10) is associated with a lower yield of secondary electron emission. The greater presence of gas on the one hand but lower secondary emission on the other hand make the situation complicated, which is reflected in the different features of the current pulses. A great deal of simulation is needed to clarify these details.

One feature, however, should be pointed out because it could be quite relevant when deciding for or against the use of krypton (apart from cost). The instabilities that were very pronounced for argon operation at high current, and are also visible to some degree with 0.5 Pa of krypton (Fig. 10 top), seem to be significantly dampened by increased krypton pressure: the sustained self-sputtering currents are rather smooth (Fig. 10 bottom). It is well known in plasma physics that collisions dampen many types of waves and instabilities. The details of the specific type of instabilities and the type of dampening collisions remain to be investigated in the future.

3.11 Gasless HIPIMS

Process gas like argon is commonly needed to ignite and maintain the discharge. In cases of high yield target materials, the gas can be completely replaced during magnetron operation. This has been demonstrated many years ago by shutting off the gas supply after starting the magnetron discharge [48, 67]. The gas could be altogether eliminated if an alternative mechanism of discharge ignition was provided. This has been realized using a short (20 μs) vacuum arc pulse, where the metal plasma was directed toward the magnetron target [33, 57]. Vacuum arc ions starting the sputtering process, and for some materials, like copper, the HIPIMS self-sputtering process can sustain itself without the further need for vacuum arc, gas supply, or any other form of assistance. Gasless sputtering in HIPIMS mode delivers extremely high ion currents to the substrate when the discharge is driven far beyond the threshold of self-sputtering [57]: this is a main difference to the previously demonstrated DC self-sputtering [48, 67]. Gasless sputtering allows us to study the magnetron self-sputtering process in its purest form, without the need to consider collisions with gas, and this helps us to study the role of secondary electron emission, effects of gas rarefaction, and the distribution of the electrical potential [44, 58].

4. Summary and concluding remarks

HIPIMS has reached a certain level of maturity as a technology. The underlying mechanisms of operation are generally understood, although many features still lack a detailed description. Examples include the time dependent potential distribution, the role of multiply charged ions versus UV photons for the emission of secondary electrons, and the type of plasma instabilities. These parameters affect the state of the plasma, the transport of plasma ions to the substrate, and ultimately the rate of and assistance to film growth. The basic operation was outlined here, including the confinement and "recycling" of energetic electrons that facilitate ionization of the gas and sputtered atoms. Experimental data suggest that target materials of high sputter yield, like copper, can operate in a sustained gasless mode whereas materials of modest sputter yield, like niobium, require the presence of some gas, usually argon. If driven to high current by high applied voltage, the discharge with target materials of modest or low sputter yield tends to develop instabilities, especially when the gas pressure is low. It was argued that the emission of secondary electrons is the key mechanism for supplying energy to the HIPIMS plasma. Replacing the gas plasma with metal plasma reduces the emission of secondary electrons, which

is likely the most important factor that terminates the runaway phase and establishes sustained self-sputtering.

Acknowledgements

Technical support by Günter Mark of Melec GmbH and Joe Wallig of Berkeley Lab is gratefully acknowledged. Joakim Andersson, David Horwat, Sunnie Lim, Jason Sanders, and Rueben Mendelsberg have been involved in experiments and/or discussions; Jonathan Slack kindly supplied figure 1. This work was supported by Berkeley Lab's LDRD program, and by the U.S. Department of Energy under Contract No. DE-AC02-05CH11231.

References

[1] V. Kouznetsov, K. Macak, J.M. Schneider, U. Helmersson, I. Petrov, Surf. Coat. Technol. 122 (1999) 290.
[2] U. Helmersson, M. Lattemann, J. Bohlmark, A.P. Ehiasarian, J.T. Gudmundsson, Thin Solid Films 513 (2006) 1.
[3] K. Sarakinos, J. Alami, S. Konstantinidis, Surf. Coat. Technol. 204 (2010) 1661.
[4] A.P. Ehiasarian, J.G. Wen, I. Petrov, J. Appl. Phys. 101 (2007) 054301.
[5] A. Ehiasarian, Fundamentals and applications of HIPIMS, in: Plasma Surface Engineering Research and its Practical Applications, R. Wei (Ed.), Research Signpost, Kerala, India, 2008, p. 35.
[6] D.M. Mattox, The history of vacuum coating technology, Society of Vacuum Coaters, Albuquerque, 2002.
[7] W.R. Grove, Phil. Mag. (1852) 498.
[8] A.W. Wright, Am. J. Science & Arts, 3rd Series 13 (1877) 49.
[9] M.J. Druyvesteyn, F.M. Penning, Rev. Mod. Phys. 12 (1940) 87.
[10] F.F. Chen, Plasma Physics and Controlled Fusion, Plenum Press, New York, 1984.
[11] F.M. Penning, Physica 3 (1939) 873.
[12] S.M. Rossnagel, H.R. Kaufman, J. Vac. Sci. Technol. A 5 (1987) 88.
[13] D.V. Mozgrin, I.K. Fetisov, G.V. Khodachenko, Plasma Phys. Rep. 21 (1995) 400.
[14] S.P. Bugaev, N.N. Koval, N.S. Sochugov, A.N. Zakharov, in: S. Anders, A. Anders (Eds.), XVIIth Int. Symp. Discharges and Electrical Insulation in Vacuum, LBNL, Berkeley, CA, 1996, p. 1074.
[15] I.K. Fetisov, A.A. Filippov, G.V. Khodachenko, D.V. Mozgrin, A.A. Pisarev, Vacuum 53 (1999) 133.
[16] A. Anders, Thin Solid Films 502 (2006) 22.
[17] A. Anders, Cathodic Arcs: From Fractal Spots to Energetic Condensation, Springer, New York, 2008.
[18] S. Schiller, K. Goedicke, J. Reschke, V. Kirchhoff, S. Schneider, F. Mildea, Surf. Coat. Technol. 61 (1993) 331.
[19] A. Belkind, A. Freilich, R. Scholl, J. Vac. Sci. Technol. A 17 (1999) 1934.
[20] S. Konstantinidis, J.P. Dauchot, M. Ganciu, A. Ricard, M. Hecq, J. Appl. Phys. 99 (2006) 013307.
[21] A. Anders, J. Andersson, A. Ehiasarian, J. Appl. Phys. 102 (2007) 113303.
[22] J. Alami, K. Sarakinos, F. Uslu, M. Wuttig, J. Phys. D: Appl. Phys. 42 (2009) 015304.

[23] K. Burcalova, et al., J. Phys. D: Appl. Phys. 41 (2008) 115306.
[24] A.P. Ehiasarian, R. New, W.-D. Münz, L. Hultman, U. Helmersson, V. Kouznetsov, Vacuum 65 (2002) 147.
[25] A.P. Ehiasarian, Y.A. Gonzalvo, T.D. Whitmore, Plasma Processes and Polymers 4 (2007) S309.
[26] A. Anders, J. Vac. Sci. Technol. A 28 (2010) 783.
[27] M. Hala, N. Viau, O. Zabeida, J.E. Klemberg-Sapieha, L. Martinu, J. Appl. Phys. 107 (2010) 043305.
[28] R. Chistyakov, B. Abraham, W.D. Sproul, 49th Ann. Tech. Conf. Proc., Society of Vacuum Coaters, Washington, D.C., 2006, p. 88.
[29] G.Y. Yushkov, A. Anders, IEEE Trans. Plasma Sci. (2010) accepted.
[30] R. Schade, Zeitschrift für Physik 104 (1937) 487.
[31] S.P. Bugaev, N.S. Sochugov, Surf. Coat. Technol. 131 (2000) 474.
[32] J. Lin, J.J. Moore, W.D. Sproul, B. Mishra, J.A. Rees, Z. Wu, R. Chistyakov, B. Abraham, Surf. Coat. Technol. 203 (2009) 3676.
[33] J. Andersson, A. Anders, Appl. Phys. Lett. 92 (2008) 221503.
[34] M. Steenbeck, Wiss. Veröff. Siemens-Konzern 9 (1930) 42.
[35] S.M. Rossnagel, J. Vac. Sci. Technol. A 6 (1988) 19.
[36] S.M. Rossnagel, J. Vac. Sci. Technol. B 16 (1998) 3008.
[37] F. Jimenez, S.D. Ekpe, S.K. Dew, J. Vacuum Sci. Technol. A 24 (2006) 1530.
[38] A. Kersch, W. Morokoff, C. Werner, J. Appl. Phys. 75 (1994) 2278.
[39] G.M. Turner, J. Vac. Sci. Technol. A 13 (1995) 2161.
[40] P. Sigmund, Phys. Rev. 184 (1969) 383.
[41] M.W. Thompson, Phil. Mag. 18 (1968) 377
[42] H. Gnaser, Energy and angular distributions of sputtered species, in: Sputtering by Particle Bombardment, R. Behrisch, W. Eckstein (Eds.), Springer, Berlin, 2007, p. 231.
[43] A. Anders, J. Andersson, A. Ehiasarian, J. Appl. Phys. 103 (2008) 039901.
[44] D. Horwat, A. Anders, J. Appl. Phys. (2011) submitted.
[45] W.D. Hoffman, J. Vac. Sci. Technol. A 3 (1985) 561.
[46] J.T. Gudmundsson, J. Alami, U. Helmersson, Surf. Coat. Technol. 161 (2002) 249.
[47] K.B. Gylfason, J. Alami, U. Helmersson, J.T. Gudmundsson, J. Phys. D: Appl. Phys. 38 (2005) 3417.
[48] N. Hosokawa, T. Tsukada, H. Kitahara, Proc. 8th Int. Vacuum Congress, Le Vide, Cannes, France, 1980, p. 11.
[49] A. Anders, Appl. Phys. Lett. 92 (2008) 201501.
[50] H. Winter, F. Aumayr, G. Lakits, Nucl. Instrum. Meth. Phys. Res. B 58 (1991) 301.
[51] H. Winter, H. Eder, F. Aumayr, J. Lorincik, Z. Sroubek, Nucl. Instrum. Meth. Phys. Res. B 182 (2001) 15.
[52] H. Eder, W. Messerschmidt, H. Winter, F. Aumayr, J. Appl. Phys. 87 (2000) 8198.
[53] A.V. Phelps, Z.L. Petrovic, Plasma Sources Sci. Technol. 8 (1999) R21.
[54] R.A. Baragiola, E.V. Alonso, J. Ferron, A. Oliva-Florio, Surf. Sci. 90 (1979) 240.
[55] J.T. Gudmundsson, P. Sigurjonsson, P. Larsson, D. Lundin, U. Helmersson, J. Appl. Phys. 105 (2009) 123302.
[56] P. Sigurjonsson, J.T. Gudmundsson, J. Phys.: Conf. Series 100 (2008) 062018.
[57] J. Andersson, A. Anders, Phys. Rev. Lett. 102 (2009) 045003.
[58] D. Horwat, A. Anders, Phys. Rev. Lett. (2011) under review.

[59] N. Brenning, I. Axnas, M.A. Raadu, D. Lundin, U. Helmersson, Plasma Sources Sci. Technol. 17 (2008) 045009.
[60] Y.W. Choi, M. Bowden, K. Muraoka, Jpn. J. Appl. Phys. 35 (1996) 5858.
[61] K.-U. Riemann, J. Phys. D: Appl. Phys. 24 (1991) 493.
[62] A.E. Wendt, M.A. Lieberman, J. Vac. Sci. Technol. A 8 (1990) 902.
[63] D. Lundin, U. Helmersson, S. Kirkpatrick, S. Rohde, N. Brenning, Plasma Sources Sci. Technol. 17 (2008) 025007.
[64] T.E. Sheridan, J. Goree, J. Vac. Sci. Technol. A 7 (1989) 1014.
[65] J. Andersson, A.P. Ehiasarian, A. Anders, Appl. Phys. Lett. 93 (2008) 071504.
[66] E. Oks, A. Anders, J. Appl. Phys. 105 (2009) 093304.
[67] W.M. Posadowski, Z. Radzimski, J. Vac. Sci. Technol. A 11 (1993) 2980.

Figure Captions

Fig. 1 Illustration of a planar magnetron similar to the one used to produce the current pulse examples in this publication.

Fig. 2 Illustration of rarefaction of argon density in magnetron sputtering. The data show the example of gas density reduction in front of the target as a function of DC power density for the case of 15 cm diameter copper target in 4 Pa of argon. The line is an extrapolation to peak power densities typical for HIPIMS: we should expect very strong rarefaction.

Fig. 3 Discharge current as a function of time for a pulsed applied voltage of 510 V (constant during on-time of 1 ms), with the time from the beginning of the pulsing experiment as a parameter (5 cm diameter niobium target, argon gas at 0.66 Pa).

Fig. 4 View of a magnetron with 5 cm diameter copper target showing evidence of melting in the center. On the right one can see a miniature cathodic arc source which is used for experiments on gasless sputtering.

Fig. 5 Illustration of self-sputtering, including the conditions for runaway and the establishment of steady-state, sustained self-sputtering.

Fig. 6 Measurement of the onset of self-sputtering near the threshold for runaway; niobium target in 0.25 Pa of argon. The applied voltage pulse is the parameter (constant during the pulse) and each curve was taken 90 s after the experiment started with a room temperature target.

Fig. 7 More examples of discharge current pulses near the runaway threshold, here taken with 520 V pulses. All other conditions are the same as indicated in Fig. 3.

Fig. 8 Current and voltage indicating the development of noise, waves, and instabilities as the HIPIMS pulses progresses; the current curve corresponds to “after 10 s” shown in Fig. 7 (5 cm diameter niobium target in 0.66 Pa of argon).

Fig. 9 Current pulses near the threshold for self-sputtering runaway; the curves may vary somewhat from pulse to pulse, though the delayed onset for applied voltages of 530 V and 540 V are reproducible (5 cm diameter niobium target in 0.5 Pa of argon).

Fig. 10 Compilation of current pulses near the threshold of self-sputtering runaway for two different pressures of krypton: top 0.5 Pa, and bottom 1.0 Pa (5 cm diameter niobium target).

Tables

Table 1. Atomic mass, work function, and first and second ionization energies for selected materials.

	m_u (a.m.u.)	ϕ (eV)	$E_{0\to1}$ (eV)	$E_{1\to2}$ (eV)
Cu	63.5	4.9	7.73	20.29
Ti	47.9	4.3	6.82	13.58
Nb	92.9	4.3	6.76	14.32
Ar	40.0	n/a	15.76	27.63
Kr	83.8	n/a	14.00	24.36

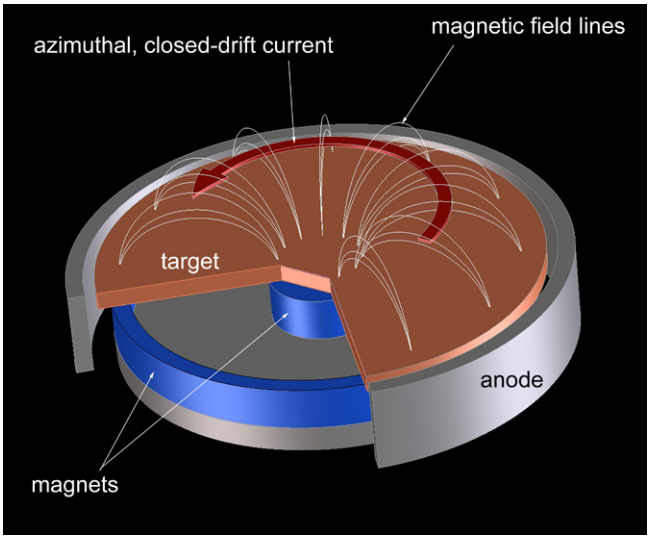
azimuthal, closed-drift current
magnetic field lines
target
anode
magnets

Fig. 1

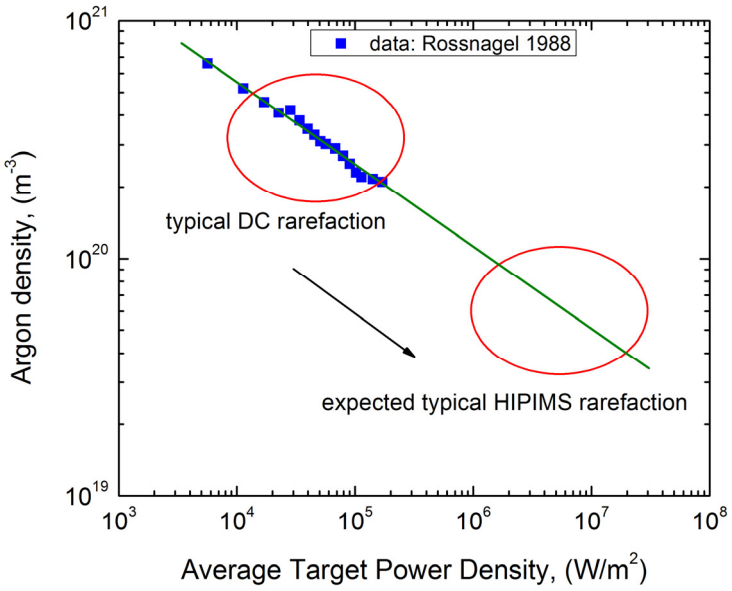
data: Rossnagel 1988
typical DC rarefaction
expected typical HIPIMS rarefaction
Argon density, (m-3)
Average Target Power Density, (W/m2)
10^21
10^20
10^19
10^3
10^4
10^5
10^6
10^7
10^8

Fig. 2

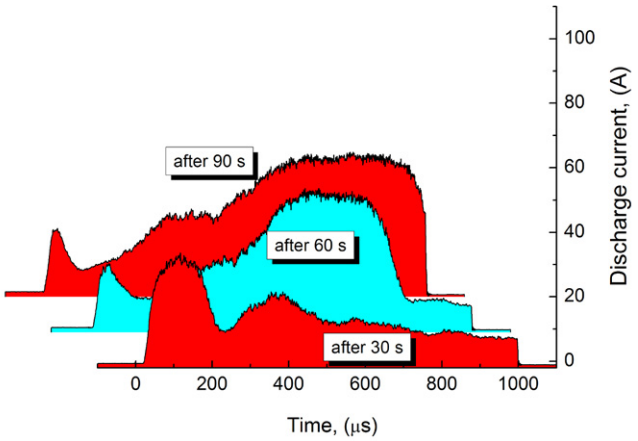
after 90 s
after 60 s
after 30 s
0
200
400
600
800
1000
Time, (μs)
0
20
40
60
80
100
Discharge current, (A)

Fig. 3

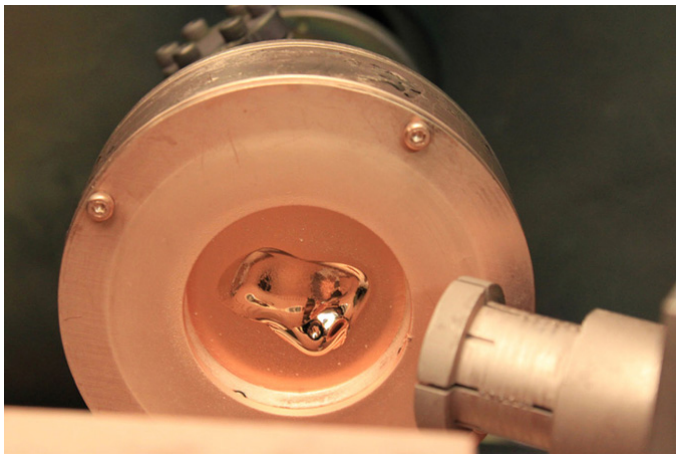

Fig. 4

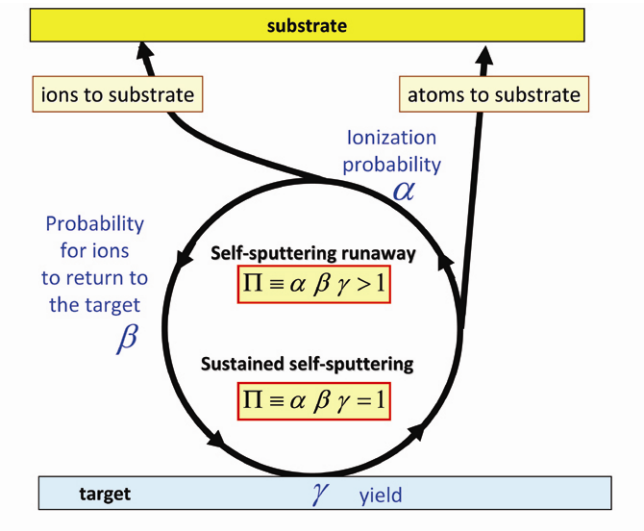
substrate
ions to substrate
atoms to substrate
Ionization probability
α
Probability for ions to return to the target
β
Self-sputtering runaway
$\Pi \equiv \alpha\ \beta\ \gamma > 1$
Sustained self-sputtering
$\Pi \equiv \alpha\ \beta\ \gamma = 1$
target
γ yield

Fig. 5

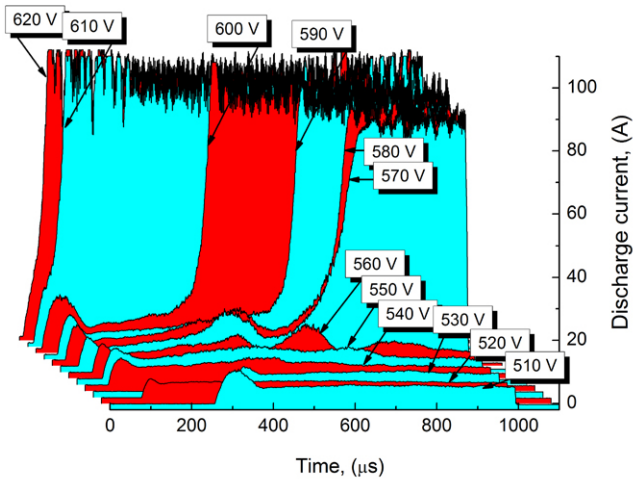
620 V
610 V
600 V
590 V
580 V
570 V
560 V
550 V
540 V
530 V
520 V
510 V
0
200
400
600
800
1000
Time, (μs)
0
20
40
60
80
100
Discharge current, (A)

Fig. 6

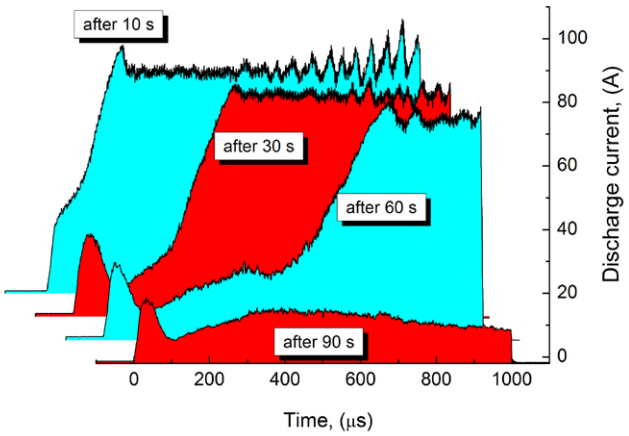
after 10 s
after 30 s
after 60 s
after 90 s
0
200
400
600
800
1000
Time, (μs)
0
20
40
60
80
100
Discharge current, (A)

Fig. 7

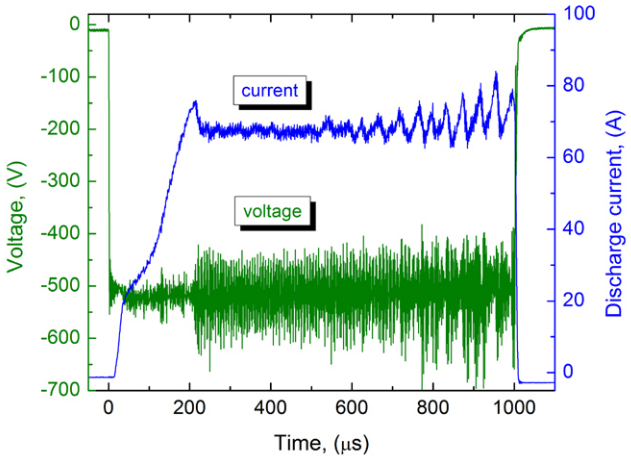
current
voltage
Voltage, (V)
Discharge current, (A)
Time, (μs)
0
-100
-200
-300
-400
-500
-600
-700
100
80
60
40
20
0
0
200
400
600
800
1000

Fig. 8

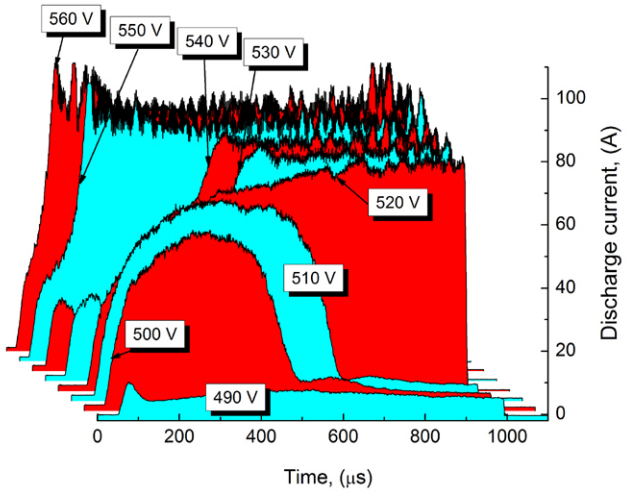
560 V
550 V
540 V
530 V
520 V
510 V
500 V
490 V
0
200
400
600
800
1000
Time, (μs)
0
20
40
60
80
100
Discharge current, (A)

Fig. 9

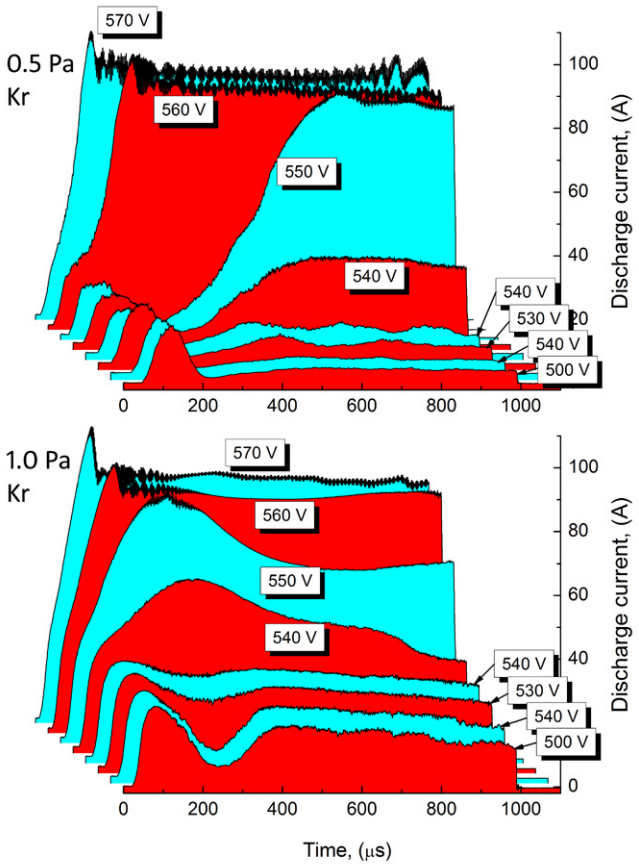
0.5 Pa
Kr
570 V
560 V
550 V
540 V
540 V
530 V
540 V
500 V
1.0 Pa
Kr
570 V
560 V
550 V
540 V
540 V
530 V
540 V
500 V
Discharge current, (A)
Time, (μs)
0
200
400
600
800
1000
0
20
40
60
80
100

Fig. 10